A small radius hydrogen discharge: An effective source of volume produced negative ions

ARTICLE *in* JOURNAL OF APPLIED PHYSICS · MAY 2010

Impact Factor: 2.18 · DOI: 10.1063/1.3369277 · Source: IEEE Xplore

3 AUTHORS, INCLUDING:

Antonia Shivarova
Sofia University "St. Kliment Ohridski"
149 PUBLICATIONS **1,273** CITATIONS

A small radius hydrogen discharge: An effective source of volume produced negative ions

Ts. Paunska,[1] A. Shivarova,[1,a)] and Kh. Tarnev[2]
[1]*Faculty of Physics, Sofia University, BG-1164 Sofia, Bulgaria*
[2]*Department of Applied Physics, Technical University–Sofia, BG-1000 Sofia, Bulgaria*

(Received 6 November 2009; accepted 18 February 2010; published online 19 April 2010)

Free-fall regime maintenance of hydrogen discharges is analyzed based on numerical solutions of a set of equations involving the balance equations of the charged particles [electrons, the three types of the positive ions (H^+, H_2^+, and H_3^+), and negative H^- ions] and of the neutral species (hydrogen atoms H and vibrationally excited molecules), the momentum equations of the positive ions, the electron energy balance equation, and the Poisson equation, all together 25 differential equations. The obtained results for varying discharge radius show strong accumulation of the negative ions in the on-axis region of the discharge when the discharge radius is small, which leads to a concept for a design of a volume-production based source as a matrix of small radius discharges. The variation in the negative ion density with changing gas pressure and electron density at the discharge axis is also analyzed. © *2010 American Institute of Physics*. [doi:10.1063/1.3369277]

I. INTRODUCTION

The current work in fusion forces active research on the rf sources of negative hydrogen ions for neutral beam injection plasma heating. As it is known,[1] the production of the negative hydrogen ions is via volume processes based on dissociative attachment of electrons to vibrationally excited molecules and via surface processes using cesium as a low work function material. The commonly accepted opinion is that the volume-production based rf source of negative hydrogen ions is the most proper solution with advantages compared to the dc discharge (filament) sources, concerning the type of the discharge, and compared to the surface production based sources, concerning the manner of the negative ion production. However, the rf source in its present design of a large-scale two-chamber source does not ensure efficiency high enough for volume production of the ions, and currently it is considered as a source with surface production of the ions.[2–4]

The design of the rf sources of negative hydrogen ions is based on the experience accumulated during many years of work on the dc filament sources[5–14] starting in the 1980s, the time when the idea for the tandem type of the source arouse. The idea is for a design that ensures spatial separation in the source of two regions, respectively, of high- and low electron temperature, and it originates from the conclusion that such a design provides conditions favoring the two-step reaction of the volume production of the negative ions: excitation of the molecules to highly vibrationally excited states that requires high-energetic electrons and production of negative ions via dissociative attachment of electrons to the vibrationally excited molecules that requires low-energetic electrons. Conclusions based on conditions favoring elementary processes in the discharge involve an assumption for locality of the discharge behavior. In the filament source this is reliable: a one-chamber source with axially homogeneous plasma just till the magnetic filter for electron cooling and drop in the electron temperature and in the electron density in the filter region, however, starting from the high value of the plasma density before the filter. This is not the case of the rf source. The source is with a two-chamber discharge vessel, and the second large-size chamber where the magnetic filter is located is a volume for plasma expansion from the driver. In such a source the conditions are strongly nonlocal, determined by the transport processes, as it has been shown recently[15–17] both by modeling and experiments.

Thus, the design of an effective rf source for volume production of the negative hydrogen ions is an open question. The results presented here, showing that the active part of the discharge—the region of the rf power deposition—provides strong accumulation of negative hydrogen ions in the on-axis region of the discharge when its radius is small, lead to a concept for a design of the source as a matrix of small radius discharges.

The study, being an extension of a recent model[18] of free-fall-regime maintained hydrogen discharges, treats a single discharge within the fluid-plasma model. Balance equations of the charged particles, hydrogen atoms and vibrationally excited hydrogen molecules, momentum equations of the positive ions, the electron energy balance, and the Poisson equation complete the initial set of equations. The radial variations of the plasma parameters are the results from the model. Their analysis stresses on the changes in the radial profile of the concentration of the negative ions with the discharge radius variation and shows that a small radius discharge sustains high concentration of negative ions in its on-axis region. This is due to a strong flux of negative ions, which are produced all over the discharge cross section, toward the discharge axis in the radial dc electric field formed in the discharge and to the possibility for the negative ions to reach the discharge center when the discharge radius is small. With the increase in the discharge radius the source

a)Electronic mail: ashiva@phys.uni-sofia.bg.

loses its efficiency. The dependence of the concentration of the negative ions on the gas pressure and on the electron density is also analyzed.

II. BASIS OF THE MODEL

Free-fall regime maintenance of hydrogen discharges in gas discharge vessels with cylindrical geometry is considered within one-dimensional (1D) model providing results for the radial discharge structure.

Electrons, the three types of positive ions (H^+, H_2^+, and H_3^+), negative ions (H^-), hydrogen atoms (H), and vibrationally excited molecules [$H_2(v)$ with $v=1-14$] are the species in the discharge involved in the model with their balance equations,

$$\frac{\partial n_e}{\partial t} + \vec{\nabla}\cdot\vec{\Gamma}_e = \frac{\delta n_e}{\delta t}, \tag{1a}$$

$$\frac{\partial n_j}{\partial t} + \vec{\nabla}\cdot\vec{\Gamma}_j = \frac{\delta n_j}{\delta t}, \tag{1b}$$

$$\frac{\partial n_n}{\partial t} + \vec{\nabla}\cdot\vec{\Gamma}_n = \frac{\delta n_n}{\delta t}, \tag{1c}$$

$$\frac{\partial N_2(v)}{\partial t} + \vec{\nabla}\cdot\vec{\Gamma}_v = \frac{\delta N_2(v)}{\delta t}, \tag{1d}$$

$$\frac{\partial N_1}{\partial t} + \vec{\nabla}\cdot\vec{\Gamma}_1 = \frac{\delta N_1}{\delta t}, \tag{1e}$$

where n_α and Γ_α are the densities and the fluxes of the charged particles, with $\alpha=e$ for electrons, $\alpha=j$ $(j=1,2,3)$ for the positive ions (respectively, H^+, H_2^+, and H_3^+), and $\alpha=n$ for the negative ions; N_1, Γ_1, $N_2(v)$ and Γ_v are the densities and the fluxes of the hydrogen atoms and of the vibrationally excited molecules. In fact, Eq. (1d) represents 14 equations for each of the vibrationally excited states ($v=1-14$) of the ground electronic state of the hydrogen molecule.

The electron flux and the negative ion flux,

$$\vec{\Gamma}_e = -b_e n_e \vec{E}_{dc} - D_e \vec{\nabla} n_e - D_e^T n_e \frac{\vec{\nabla} T_e}{T_e}, \tag{2a}$$

$$\vec{\Gamma}_n = -b_n n_n \vec{E}_{dc} - D_n \vec{\nabla} n_n, \tag{2b}$$

are drift-diffusion fluxes with thermal diffusion taken into account in the electron flux. Here $\vec{E}_{dc}=-\vec{\nabla}\Phi$ is the intensity of the dc electric field formed in the discharge, with Φ being its potential and T_e being the electron temperature (in energy units). The electron mobility b_e and diffusion coefficient D_e as well as the thermal diffusion coefficient $D_e^T \equiv D_e$ are defined via the frequencies of the elastic collisions of electrons with atoms and molecules, whereas the mobility b_n and the diffusion coefficient D_n of the negative ions are effective ones accounting also for the inelastic collisions for their production. The fluxes of the neutral species are diffusion fluxes,

$$\vec{\Gamma}_1 = -D_1 \vec{\nabla} N_1, \tag{2c}$$

$$\vec{\Gamma}_v = -D_v \vec{\nabla} N_2(v), \tag{2d}$$

with D_1 and D_v being the corresponding diffusion coefficients.

For the determination of the fluxes $\vec{\Gamma}_j$ $(j=1-3)$ of the positive ions, their momentum equations are solved with account for the nonlinear inertia term, as necessary for description of discharge maintenance in a free-fall regime,

$$m_j n_j \left[\frac{\partial \vec{v}_j}{\partial t} + (\vec{v}_j \cdot \vec{\nabla})\vec{v}_j \right] = e n_j \vec{E}_{dc} - \kappa T_j \vec{\nabla} n_j - \sum_{k=1}^{2} \mu_{j-k} \nu_{j-k} n_j \vec{v}_j - m_j \vec{v}_j \frac{\delta n_j}{\delta t}. \tag{2e}$$

Here m_j and v_j are the masses and the velocities of the positive ions, e is the elementary charge, μ_{j-k} are the reduced masses in elastic ion-neutral collisions, with frequencies ν_{j-k} for collisions with atoms and molecules ($k=1$ and 2 for H and H_2), and the last term in Eq. (2e) that accounts for the inelastic collisions for production of the ions also specifies low-pressure discharge description; T_j is the temperature of the positive ions and κ is the Boltzmann constant. As Eq. (2e) shows, whereas the dc electric field, directed toward the discharge walls accelerates the positive ions towards the walls, the inertia term, the second term in the left-hand side, acts as a retarding force that limits the increase of the ion velocity close to the walls.

In the electron energy balance

$$\frac{3}{2}\frac{\partial}{\partial t}(n_e T_e) + \text{div}\, \vec{J}_e = P_w - P_{coll} - e\vec{\Gamma}_e \cdot \vec{E}_{dc}, \tag{3}$$

$$\vec{J}_e = -\chi_e \vec{\nabla} \vec{\Gamma}_e + \frac{5}{2} T_e \vec{\Gamma}_e \tag{4}$$

is the electron energy flux including both the conductive flux (with χ_e being the thermal conductivity coefficient) and the convective flux [respectively, the first and second terms in the right hand side of Eq. (4)], P_w is the rf power density deposition applied for the discharge maintenance, assumed to be radially constant, P_{coll} is the electron energy losses in collisions and the last term accounts for electron energy losses for maintenance of the dc electric field in the discharge. The losses in collisions are in elastic collisions with atoms and molecules and in inelastic collisions for ionization, excitation (of the first four levels) and ionization of the atoms, dissociation of the molecules, and their excitation to the first two vibrationally excited states of the ground electronic state and to the singlet ($B\ ^1\Sigma_u^+$, $C\ ^1\Pi_u$, and $E,F\ ^1\Sigma_g^+$) states.

The Poisson equation

$$\Delta\Phi = -\frac{e}{\varepsilon_0}\left(\sum_{j=1}^{3} n_j - n_e - n_n \right) \tag{5}$$

couples the potential Φ of the dc electric field formed in the discharge to the charged particle densities; ε_0 is the vacuum permittivity.

TABLE I. Processes for production of positive and negative ions and hydrogen atoms.

No.	Process	Reference
1	$e+H_2 \rightarrow H_2^+ + e + e$	19
2	$e+H_2 \rightarrow H + H + e$	19
3	$e+H_2^+ \rightarrow e + H^+ + H\ (1s)$	19
4	$H_2^+ + H_2 \rightarrow H_3^+ + H\ (1s)$	20
5	$e+H\ (1s) \rightarrow H^+ + e + e$	19
6	$e+H_3^+ \rightarrow H + H + H$	19
7	$e+H_3^+ \rightarrow e + H^+ + 2H$	19
8	$e+H_2(v=4-9) \rightarrow H^- + H$	21
9	$e+H^- \rightarrow H\ (1s) + e + e$	19
10	$e+H^- \rightarrow e + H^+ + 2e$	19
11	$H^+ + H^- \rightarrow H + H$	22
12	$H_2^+ + H^- \rightarrow H + H_2$	22
13	$H_3^+ + H^- \rightarrow H_2 + H_2$	22
14	$H + H^- \rightarrow H_2 + e$	22
15	$H + H_{ad} \rightarrow H_2$	23 and 24

The density of the ground state molecules is determined from the expression for the gas pressure

$$p = \kappa T_g (N_1 + N_2), \tag{6}$$

which is the last equation in the model; here T_g is the gas temperature.

The particle production and losses, i.e., the terms in the right hand side of Eqs. (1a)–(1e), are according to the reactions in Tables I and II. The references used for the determination of the rate coefficients are also given in the tables. The balance of the vibrationally excited states (Table II) includes vibrational-translational (V-T) processes with molecules and atoms (reactions 1 and 2 in Table II), vibrational-vibrational (V-V) processes [reaction (3)], and e-V and E-V collisions (reactions 4 and 5); for more details, see Ref. 18.

The boundary conditions are the ordinary ones[29,30] for symmetry on the discharge axis and for the particle fluxes at the discharge walls.

Compared to the model in Ref. 18, the improvements here concern the form of the initial set of equations and the numerical procedure. Whereas in Ref. 18 the balance equations of the charged particles, the momentum equations of the positive ions, and the electron energy balance equation are solved in their stationary form, here they are solved—by employing Comsol MULTIPHYSICS numerical environment—in their nonstationary form as partial differential equations [Eqs. (1a)–(1c), (2e), and (3)] including not only the radial variation but also the time dependence. This permits direct account for the boundary conditions instead of determining the electron temperature in iterations until having the conditions for the fluxes at the discharge walls fulfilled, as it has been done before.[18] Also the balance equations of the vibrationally excited states [Eq. (1d)] and the balance equation of the hydrogen atoms [Eq. (1e)] are now solved as partial differential equations instead of using local balance at the discharge axis. In addition, instead of employing a rate coefficient for total production of negative ions from the (v=4–9)-excited states considered as a whole, here the H^--production is specified from each of the vibrational states separately. In Ref. 18, H^--production is considered also from the Rydberg states. However, due to the uncertainty of the value of this rate coefficient (three orders of magnitude difference in the experimental and theoretical values[31,32]), H^--production from the Rydberg states is not considered here. As the results in Ref. 18 show, accounting for negative ion production from the Rydberg states by using the high experimental value of its rate coefficient gives up to twice higher values of the negative ion density.

TABLE II. Processes involved in the balance of the vibrationally excited states of the molecules.

No.	Process	Reference
1	$H_2(v) + H_2 \leftrightarrow H_2(v-1) + H_2$	25
2	$H_2(v) + H \leftrightarrow H_2(v-1) + H$	25
3	$H_2(v+1) + H_2(w) \leftrightarrow H_2(v) + H_2(w+1)$	25
4	$e+H_2(v) \leftrightarrow e+H_2(w)\ \ (v=0-6)$	25 and 26
5	$e+H_2(v) \rightarrow e+H_2^*(B\ ^1\Sigma_u^+, C\ ^1\Pi_u) \rightarrow e+H_2(w)+h\nu$	27
6	$H_2+H_2(v=14) \rightarrow H_2+2H$	25
7	$H_2(v=14)+H_2(w+1) \rightarrow H_2(w)+2H$	25
8	$H_2(v)+\text{wall} \rightarrow H_2(v-1)+\text{wall}$	28

III. RESULTS AND DISCUSSIONS

The discussion is on the cw regime of discharge maintenance. The results presented are for the radial structure of low-pressure hydrogen discharges composed by the self-consistent variations in the concentrations of charged particles and neutral species, of the electron temperature, and of the dc electric field intensity. The discussions stress on the results for the density of the negative ions and its variation with the changes in the discharge radius. Results for the changes in the negative ion density with the gas pressure and the electron density at the discharge axis are also commented on.

The gas pressure values considered are in the millitorr range. The radius of the gas discharge tube is varied between 2 and 10 cm. The variation in the electron density at the discharge axis is in the range of $n_e=(1\times10^{10}-8\times10^{11})$ cm^{-3}. The other external parameters are $T_j=T_g=400$ K and $T_n=1000$ K. The analysis of the results aims at conclusions for the use of the discharge as a source of volume produced negative hydrogen ions.

A. Changes in the radial structure of low-pressure hydrogen discharges with the variation in the discharge radius

The results in this subsection are for given values of the gas pressure ($p=7.5$ mTorr) and of the electron concentration at the discharge axis ($n_{e0}\equiv n_e(r=0)=3.5\times10^{11}$ cm^{-3}) and different values of the discharge radius in the range of $R=(2-10)$ cm.

The obtained profiles of the densities of the negatively charged particles—electrons and negative hydrogen ions—are respectively in Figs. 1(a) and 1(b).

The radial profiles of the electron density [Fig. 1(a)] show well pronounced wall sheath, typical for the free-fall regime of discharge maintenance. According to the expecta-

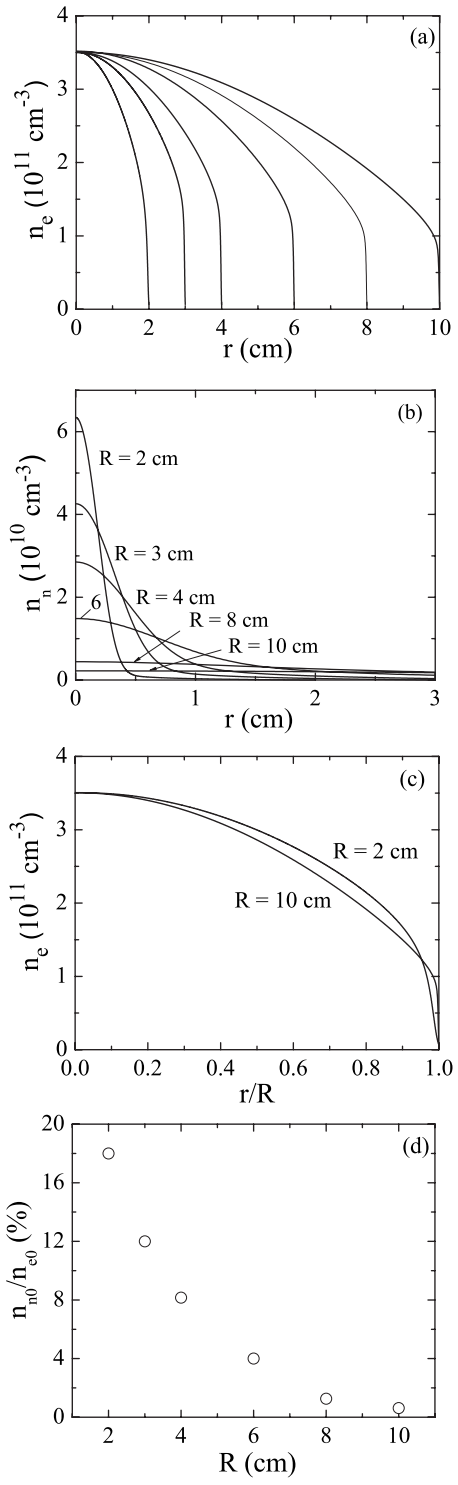

FIG. 1. Radial profiles of the concentrations of electrons (a) and negative hydrogen ions (b) for different values of the discharge radius as denoted in (b) and marked by the ends of the profiles in (a) as well as variation in the electron density over the normalized radius (r/R) for $R=2$ cm and $R=10$ cm in (c). In (d), the ratio of the concentrations of the negative ions and of the electrons at the discharge center is given for different values of the discharge radius; $p=7.5$ mTorr and $n_{e0} \equiv n_e(r=0)=3.5\times10^{11}$ cm^{-3}. The r-axis in (b) is cut at $r=3$ cm.

tions, for a given value of the gas pressure, the free-fall regime is better pronounced for smaller values of the discharge radius. This is demonstrated by Fig. 1(c), which shows the flattening—typical for a free-fall regime—of the radial profile of the electron density. The decrease in the electron density over the normalized radius (r/R) is slower for $R=2$ cm than for $R=10$ cm [Fig. 1(c)], and the wall sheath is wider. The widening of the wall sheath with decreasing discharge radius is also evident in the results for the radial profiles of the potential of the dc electric field in the discharge, not shown here.

Regarding the aim of the study, directed toward determining conditions proper for a design of a volume-production based source of negative hydrogen ions, Figs. 1(b) and 1(d) show key results. Presenting radial profiles of the concentration of the negative ions, Fig. 1(b) demonstrates strong accumulation of the negative ions in the on-axis region of the discharge when the discharge radius is small. For the given values of the gas pressure and of the electron density at the discharge axis, the ratio of the concentrations of the negative ions and of the electrons falls down from about 18% to about 0.6% [Fig. 1(d)] when the discharge radius increases from 2 to 10 cm. The latter value of R is close to that of the driver of the two-chamber rf source[2–4] currently developed for fusion applications. The results show that whereas a large diameter driver does not ensure efficient production of negative ions, thus requiring looking for a solution via extension of the discharge vessel of the source to a two-chamber tandem type of a source, the simple construction of a small radius driver provides high negative hydrogen ion density. This result traces out a concept for a design of an effective volume-production based source of negative hydrogen ions as a matrix of small radius discharges with a single hole extraction from each of them, centered at the discharge axis.

The results for the concentrations of the positive ions (Fig. 2) show a decrease in the concentration n_1 of the H^+-ions and corresponding increase in the concentration of the H_2^+-ions with the decrease in the discharge radius. In general, the H^+- and H_2^+-ions show up as dominating positive ions. The concentration of the H_3^+-ions is an order of magnitude lower for all values of the discharge radius. For the lowest value of the discharge radius ($R=2$ cm), the concentration of the H_2^+-ions prevails over that of the H^+-ions, whereas for the highest value of R ($R=10$ cm), it is the opposite. The distortion of the profiles of the ion density, with formation of bulges in the on-axis region of the discharge, is associated with the accumulation of the negative ions in the discharge center, as it has been already discussed in Ref. 18. In a way, the positive ions play the role to keep the quasineutrality in the plasma core. This distortion is well pronounced in the cases of a small discharge radius where the accumulation of the negative ions in the vicinity of the discharge axis is strong [Fig. 1(b)], and it disappears for large R, cases where the negative ion density profiles are smooth.

Figures 3(a) and 3(b) show the radial profiles of the electron temperature T_e and of the intensity of the dc electric field E_{dc} formed in the discharge.

The electron temperature T_e is almost constant across the discharge radius. This is due rather to high thermal conductivity than to the radially constant rf power deposition in the discharge. The latter is confirmed by results obtained by specifying the rf power deposition as a power deposition to

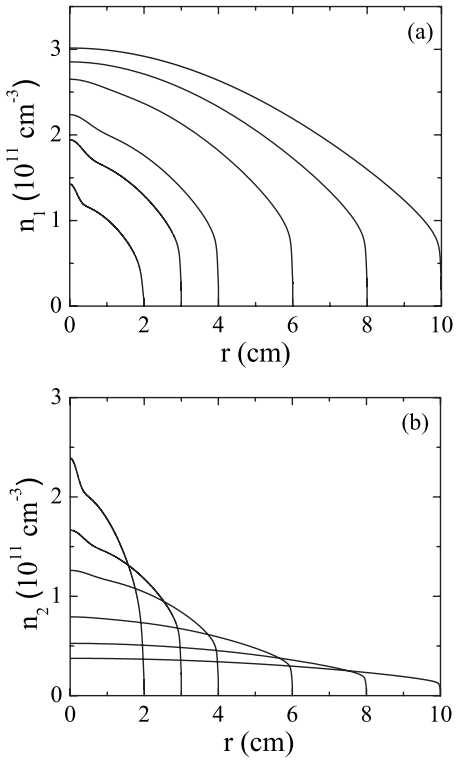

FIG. 2. Radial profiles of the concentration n_1 of the H^+-ions (a) and of the concentration n_2 of the H_2^+-ions (b) for different values of the discharge radius as marked by the ends of the profiles; p=7.5 mTorr and n_{e0}=3.5 $\times 10^{11}$ cm^{-3}.

inductive discharges with a cylindrical coil.[33] In fact, Ref. 33 presents coupling of the 1D fluid-plasma model presented here to the theory of the nonlocal electrodynamics of inductive discharges with cylindrical coils developed before[34] within the kinetic plasma theory. The electrodynamical description[33,34] is based on a solution of the wave equation written for the azimuthal electric field of the transverse high-frequency wave sustaining the inductive discharges. In accordance with the low gas pressure, the electrodynamics treats conditions of nonlocal conductivity, resulting from the anomalous skin and the reflection of the electrons by the potential barrier of the dc field in the wall sheath, and of stochastic heating of the electrons in the rf electric field. The radial profiles of the amplitudes of the high-frequency field components and of the rf power deposition show the well-known effects of the nonlocal conductivity.[35,36] However, the changes in the radial distribution of the rf power deposition do not show evidence in the radial profiles of the ion densities. Thus, the result stressed here for the accumulation of the negative ions in the on-axis region of small radius discharges, obtained within the fluid-plasma model description, stays stable and not influenced by the manner of the rf power deposition to the discharge.

The increase—with the decrease in the discharge radius—in the electron temperature shown in Fig. 3(a) and the corresponding increase in the parameter $\Theta = P_w/\bar{n}_e$ [Fig. 3(c)], the power absorbed on average—over the discharge cross section—by an electron, are due to the larger losses of charged particles for smaller discharge radius. In the case of small discharge radii the electron temperature (Fig. 3) exceeds 10 eV. Although the rate coefficient of the losses of the negative ions in collisions with electrons increases with T_e, the dependence is not so strong (an increase by a factor of 2 when T_e increases from 6 to 12 eV), and due to the higher velocity of the negative ions when the discharge radius is small, this does not cause reduction in the survival distance of the negative ions.

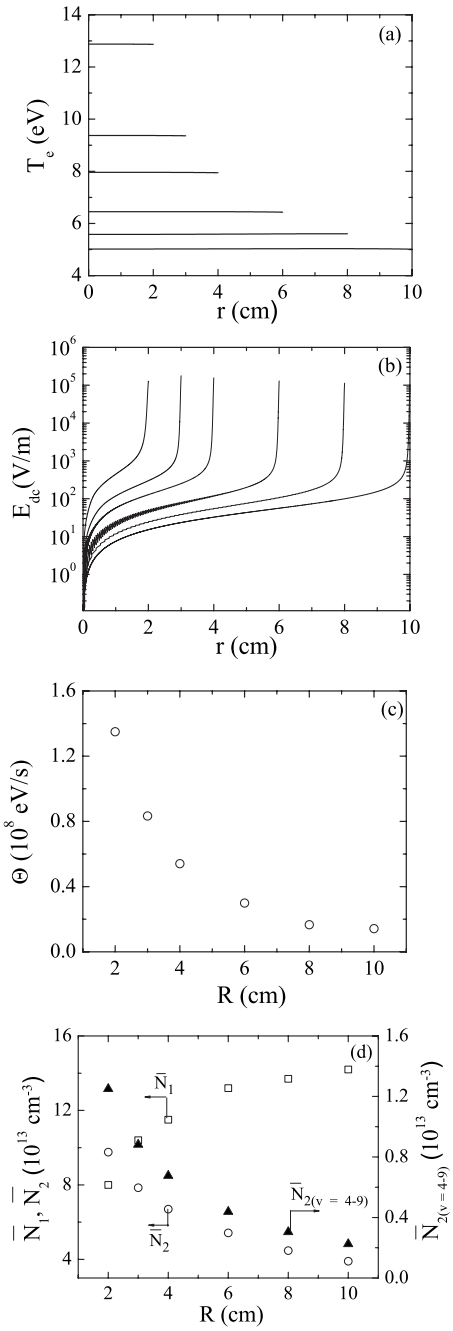

FIG. 3. Radial profiles of the electron temperature T_e (a) and of the dc electric field intensity E_{dc} (b) for different values of the discharge radius marked by the ends of the profiles. Dependence on the discharge radius R of the parameter Θ (c) and of the averaged—over the discharge cross section—concentrations of atoms ($\bar{N}_1$), molecules ($\bar{N}_2$), and vibrationally excited molecules ($\bar{N}_{2(v=4-9)}$) with v=4–9 (d); p=7.5 mTorr and n_{e0}=3.5$\times 10^{11}$ cm^{-3}.

The potential of the dc electric field formed in the discharge increases with the discharge radius decrease, determining a strong dc field intensity over the total cross section of small radius discharges [Fig. 3(b)].

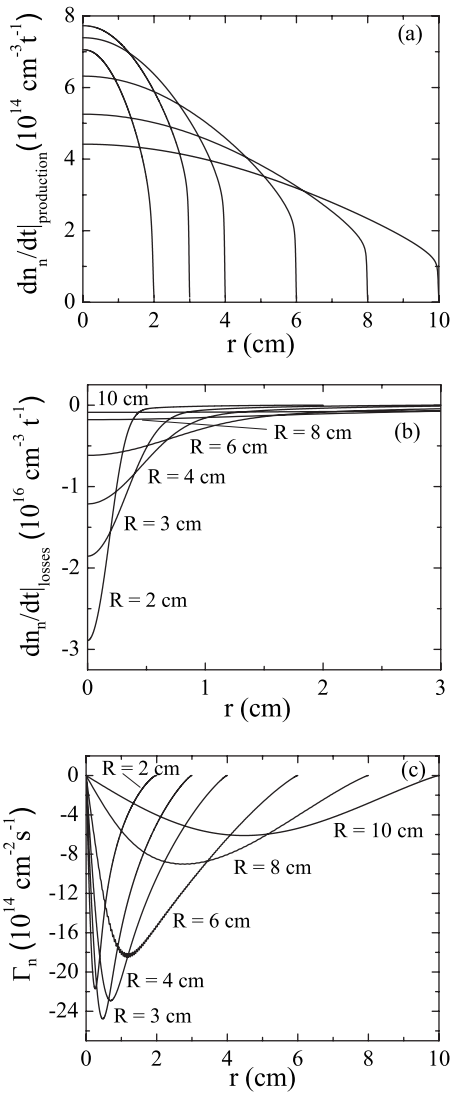

FIG. 4. Radial variation in the local production ($\delta n_n/\delta t|_{\text{production}}$) and losses ($\delta n_n/\delta t|_{\text{losses}}$) of the negative ions, respectively, in (a) and (b) as well as of the flux Γ_n of the negative ions (c) for different values of the discharge radius R as marked in (b) and (c) and by the ends of the profiles in (a). In (b), the r-axis is cut at $r=3$ cm.

The concentrations of the neutral species are almost constant across the discharge radius for all the values of R. The hydrogen atom concentration decreases, and, respectively, the concentration of the hydrogen molecules increases with the decrease in R [Fig. 3(d)]. This is in accordance with the dependence of the densities of the atomic and molecular ions on the discharge radius: higher concentration of the molecular ions for smaller radius discharges. The total concentration of the vibrationally excited molecules with vibrational quantum number v=4–9, i.e., the excited states that provide an efficient negative ion production, also increases with the decrease in the discharge radius. Respectively, the concentration of the negative ions [Figs. 1(b) and 1(d)] is higher for a smaller discharge radius.

The latter is confirmed by Fig. 4(a) that shows the radial variations of the production of the negative ions in the cases of discharges with different values of the discharge radius. With the constant value—across the discharge radius—of the density of the vibrationally excited molecules, the radial variation in the local negative ion production follows the trends of the radial variation in the electron density [Fig. 1(a)]. The case of a discharge radius of $R=3$ cm shows up with the most efficient negative ion production. The local production of the negative ions is all over the discharge cross section. With their accumulation in the on-axis region of the discharge [Fig. 1(b)], their local losses [Fig. 4(b)] are also in this region. The local losses of the negative ions strongly predominate over their local production in the on-axis region of the discharge. The reason is that the flux—in the dc electric field—of the negative ions from the outer region of the discharge towards its center [Fig. 4(c)] is the main contributor to the negative ion density in the on-axis region of the discharge leading to their accumulation there. The comparison of the fluxes for different values of the discharge radius shows that at small values of the radius ($R=2-4$ cm), the flux is four times higher than for a large discharge radius ($R=10$ cm). This is due to the stronger dc field intensity [Fig. 3(b)] in small radius discharges. The radial variation in the negative ion flux from the outer region of the discharge toward its center shows first an increase in the flux followed by its decrease (to a zero value at $r=0$). The former is due to predominating drift motion in the dc field, which forces the ions from the outer region of the discharge toward its center. However, with the accumulation of the ions in the on-axis region of the discharge, the role of the diffusion increases, forcing the ions in the opposite direction (outward from the discharge axis).

The main conclusion from the results on the discharge structure at different discharge radii is for a strong accumulation of the negative ions in the on-axis region of the discharge when its radius is small. The accumulation of the negative ions in the on-axis region of the discharge is a combined effect of the stronger dc electric field and the lower probability for their local destruction in collisions in small radius discharges. Due to the small survival distance of the negative ions, the ions produced in the outer region of the discharge can reach the discharge center only in the cases when the discharge radius is small.

B. Influence of the gas pressure variations

The results briefly commented on here are for varying gas pressure values in the range of $p=(5-10)$ mTorr and given values of the discharge radius ($R=3$ cm) and of the electron density at the discharge axis ($n_{e0}=3.5\times10^{11}$ cm^{-3}).

With the gas pressure variation the discharge behaves as it should be expected: with the gas pressure decrease, the electron temperature and potential of the dc electric field increase. The rf power density necessary for sustaining discharges with a given electron density at the discharge axis also increases. However, the redistribution of the plasma parameters with the changes in the gas pressure leads to nonmonotonic variation in the negative ion density with p (Fig. 5). Such a nonmonotonic dependence is observed also in experiments.[37,38] However, the changes in the negative ion

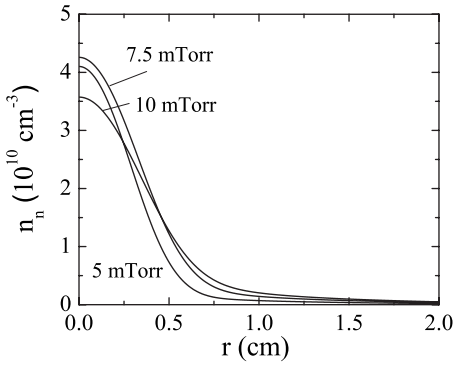

FIG. 5. Radial profiles of the concentration of the negative ions for different values of the gas pressure; $R=3$ cm and $n_{e0}=3.5\times10^{11}$ cm^{-3}. The r-axis is cut at $r=2$ cm.

density profile with the gas pressure are slight, not influencing the conclusion for a strong accumulation of the ions in the on-axis region of the discharge.

C. Influence of the electron density at the discharge axis

The electron density n_{e0} at the discharge axis is the other parameter varied in the range of $n_{e0}=(1\times10^{10}-8\times10^{11})$ cm^{-3} for given values of the discharge radius ($R=3$ cm) and of the gas pressure ($p=5$ mTorr). The results presented are mainly for the negative ion density: radial profiles [Fig. 6(a)] of the density of the ions, radial variation in the ratio of the negative ion density and the electron density [Fig. 6(b)], and changes in the ratio of the averaged—over the discharge cross section—densities of the negative ions and electrons with the variation in the electron concentration at the discharge axis [Fig. 6(c)].

The electron temperature increases with the increase in the electron concentration n_{e0} at the discharge axis [Fig. 6(d)]. This is due to an increase in the concentration of the H^+-ions with n_{e0}. Due to their high mobility, the charged particle losses increase leading to the increase in the electron temperature.

The negative ion density increases with the electron concentration n_{e0} monotonically in the range of $n_{e0}=(1\times10^{10}-4\times10^{11})$ cm^{-3} [Fig. 6(a)]. The further increase in n_{e0} leads to a decrease in n_n. Such a dependence can be related to redistribution in the contributors to the negative ion balance. At low n_{e0} the volume losses of the H^--ions are mainly due to collisions with hydrogen atoms. With the n_{e0}-increase both the production and the losses of negative ions increase. However, their production increases proportionally to n_{e0}, whereas the increase in their losses is slower due to the slow increase in N_1 with n_{e0}. As a result, the density of the negative ions increases. This is up to the n_{e0}-values for which the negative ion losses in collisions with hydrogen atoms dominate over their losses in collisions with electrons. At n_{e0}-values high enough, the collisions of the negative ions with electrons become the main mechanism of their losses. Due to their fast increase with n_{e0}, the concentration of the negative ions decreases.

Conditions of low electron density at the discharge axis show up with very high relative density of the negative ions:

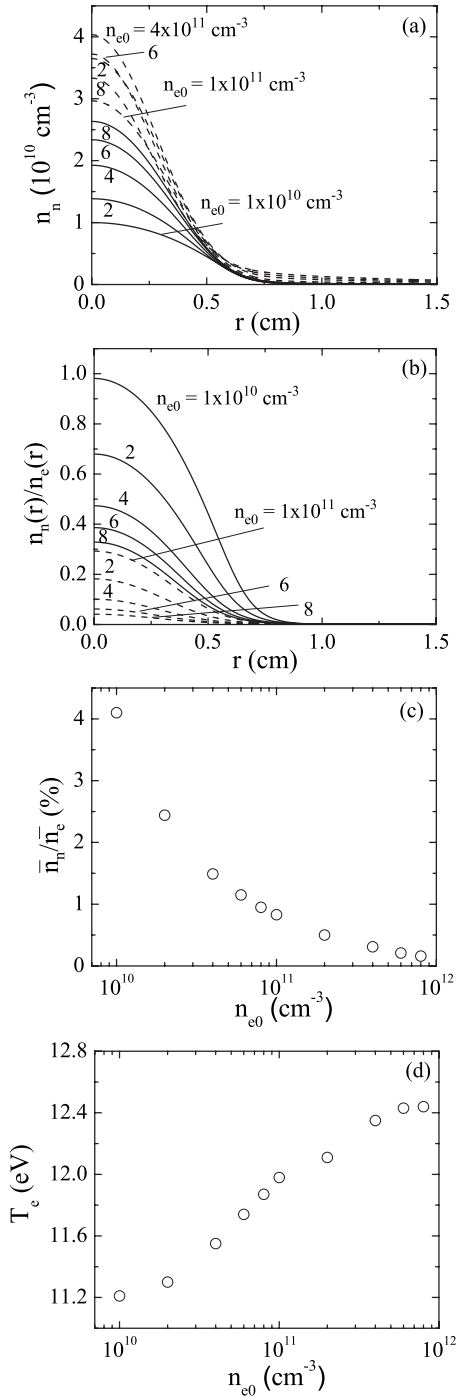

FIG. 6. Radial variation in the density of the negative ions (a) and of the ratio of their density to the electron density (b) for different values of the electron concentration n_{e0} at the discharge axis and changes in the ratio of the averaged—over the discharge cross section—densities of negative ions and electrons (c) and of the electron temperature (d) with the electron density at the discharge axis; $R=3$ cm and $p=5$ mTorr. In (a) and (b), the r-axis is cut at $r=1.5$ cm, and the values of the order of 10^{10} and 10^{11} cm^{-3} are given respectively by solid and dashed curves.

at $n_{e0}=1\times10^{10}$ cm^{-3}, the negative ion density at $r=0$ is close to that of the electrons [Fig. 6(b)]. The ratio of the averaged concentrations—over the discharge cross section—of negative ions and electrons has also its highest value for the lowest value of n_{e0} [Fig. 6(c)]. Such a result—high negative ion density accompanied by low electron density—is in the trends required for the negative ion sources in fusion.

IV. CONCLUSIONS

The study presents a 1D model of low-pressure hydrogen discharges. According to the pressure range studied, the model is for discharge maintenance in a free-fall regime. Based on the fluid-plasma theory, the initial set of equations numerically solved includes the continuity equations of electrons, of the three types of the positive ions (H^+, H_2^+, and H_3^+), of the negative ions, of the hydrogen atoms, and of the 14 vibrationally excited states of the ground electronic state of the hydrogen molecules, the momentum equations of the positive ions with the nonlinear inertia terms taken into account, the electron energy balance equation, the Poisson equation, and the equation of state.

The analysis of the results for the radial structure of the discharge shows strong accumulation of the negative ions in the discharge center when the discharge radius is small. The negative ion production is all over the discharge cross section, and their flux in the dc electric field formed in the discharge is toward the discharge axis. However, when the discharge radius is small, the electric field accelerating the ions is strong, and the probability for their destruction in collisions is low. This leads to the accumulation of the negative ions in the central region of the discharge. At comparatively low electron density (electron density of 10^{10} cm^{-3} at the discharge axis), the negative ion density is close to the electron density. These results show that the driver region of the discharge is an efficient source of volume produced negative ions, and further investigations on a design of a rf source of negative ions performed as a matrix of small radius discharges with a single hole extraction from the on-axis region of each of them seem to be reasonable.

It has been usually discussed that the volume production of the negative ions requires space separation in the source of regions of high and low electron temperature, for favoring, respectively, the two steps of the reaction of negative ion production from vibrationally excited molecules. However, the current understanding of the gas discharges calls for self-consistency of the discharge structure, which is hardly compatible with judgments on the discharge behavior based on considering isolated from the entire discharge structure two reactions in the discharge. This study shows that judgments on the capability of the sources of negative hydrogen ions and their efficiency should be based on the complete discharge structure obtained by accounting both for local and nonlocal (i.e., fluxes) processes.

ACKNOWLEDGMENTS

The work was within Project No. DO02-267 supported by the National Science Fund of Bulgaria, and it was part of the program of the Bulgarian Association EURATOM/INRNE (Task 2.1.1).

[1]J. Ishikawa, in *The Physics and Technology of Ion Sources*, edited by G. Brown (Wiley, Weinheim, 2004), p. 285.
[2]E. Speth, H. D. Falter, P. Franzen, U. Fantz, M. Bandyopadhyay, S. Christ, A. Encheva, M. Fröschle, D. Holtum, B. Heinemann, W. Kraus, A. Lorenz, Ch. Martens, P. McNeely, S. Obermayer, R. Riedl, R. Süss, A. Tanga, R. Wilhelm, and D. Wünderlich, Nucl. Fusion **46**, S220 (2006).
[3]S. Christ-Koch, U. Fantz, M. Berger, and NNBI Team, Plasma Sources Sci. Technol. **18**, 025003 (2009).
[4]P. McNeely, S. U. Dudin, S. Christ-Koch, U. Fantz, and NNBI Team, Plasma Sources Sci. Technol. **18**, 014011 (2009).
[5]M. Bacal, Nucl. Fusion **46**, S250 (2006).
[6]M. Bacal, A. M. Brunetau, and M. Nachman, J. Appl. Phys. **55**, 15 (1984).
[7]T. Inoue, M. Araki, M. Hanada, T. Kurashima, S. Matsuda, Y. Matsuda, Y. Ohara, Y. Okumura, S. Tanaka, and K. Watanabe, Nucl. Instrum. Methods Phys. Res. B **37–38**, 111 (1989).
[8]K. N. Leung, O. A. Anderson, C. F. Chan, W. S. Cooper, G. J. DeVries, C. A. Hauck, W. B. Kunkel, J. W. Kwan, A. F. Leitzke, P. Purgalis, and R. P. Wells, Rev. Sci. Instrum. **61**, 2378 (1990).
[9]F. A. Haas, L. M. Lea, and A. J. T. Holmes, J. Phys. D: Appl. Phys. **24**, 1541 (1991).
[10]O. Fukumasa, M. Hosoda, and H. Naiton, Rev. Sci. Instrum. **63**, 2696 (1992).
[11]A. J. T. Holmes, Plasma Phys. Controlled Fusion **34**, 653 (1992).
[12]G. I. Dimov, Rev. Sci. Instrum. **73**, 970 (2002).
[13]A. J. T. Holmes, R. McAdams, G. Proudfoot, S. Cox, E. Surrey, and R. King, Rev. Sci. Instrum. **65**, 1153 (1994).
[14]Y. Takeiri, A. Ando, O. Kaneko, Y. Oka, K. Tsumori, R. Akiyama, E. Asano, T. Kawamoto, T. Kuroda, M. Tanaka, and H. Kawakami, Rev. Sci. Instrum. **66**, 2541 (1995).
[15]Ts. V. Paunska, A. P. Shivarova, Kh. Ts. Tarnev, and Ts. V. Tsankov, AIP Conf. Proc. **1097**, 12 (2009).
[16]Ts. V. Paunska, A. P. Shivarova, Kh. Ts. Tarnev, and Ts. V. Tsankov, AIP Conf. Proc. **1097**, 99 (2009).
[17]St. St. Lishev, A. P. Shivarova, and Ts. V. Tsankov, AIP Conf. Proc. **1097**, 127 (2009).
[18]Ts. Paunska, H. Schlüter, A. Shivarova, and Kh. Tarnev, Phys. Plasmas **13**, 023504 (2006).
[19]R. K. Janev, W. D. Langer, K. Evans, Jr., and D. B. Post, Jr., *Elementary Processes in Hydrogen-Helium Plasmas* (Springer, Berlin, 1987).
[20]R. H. Neynaber and S. M. Trujillo, Phys. Rev. **167**, 63 (1968).
[21]D. Reiter, *Additional Atomic and Molecular Data for EIRENE* (FZ, Forschungfzentrum, Jülich GmbH, Jülich, 2004).
[22]G. M. Petrov and Tz. Petrova, Plasma Chem. Plasma Process. **22**, 573 (2002).
[23]L. St-Onge and M. Moisan, Plasma Chem. Plasma Process. **14**, 87 (1994).
[24]A. Rousseau, A. Granier, G. Gouset, and P. Leprince, J. Phys. D: Appl. Phys. **27**, 1412 (1994).
[25]J. Loureiro and C. M. Ferreira, J. Phys. D: Appl. Phys. **22**, 1680 (1989).
[26]H. Ehrhardt, L. Langhaus, F. Linder, and H. S. Taylor, Phys. Rev. **173**, 222 (1968).
[27]R. Celiberto, R. K. Janev, A. Larinchita, M. Capitelli, J. M. Wadehra, and P. E. Atems, At. Data Nucl. Data Tables **77**, 161 (2001).
[28]C. Gorse, M. Capitelli, and A. Ricard, J. Chem. Phys. **82**, 1900 (1985).
[29]J. P. Boeuf and L. C. Pitchford, Phys. Rev. E **51**, 1376 (1995).
[30]G. I. M. Hagelaar, F. S. de Hoong, and G. M. W. Kroesen, Phys. Rev. E **62**, 1452 (2000).
[31]L. A. Pinnaduwage and L. G. Christophorou, Phys. Rev. Lett. **70**, 754 (1993).
[32]J. R. Hiskes, Appl. Phys. Lett. **69**, 755 (1996).
[33]St. Kolev, Ts. Paunska, A. Shivarova, Kh. Tarnev, and Ts. Tsankov, 36th EPS Conf. on Plasma Phys. Sofia, Bulgaria, 2009 [ECA 33E, O-5.064 (2009)].
[34]St. Kolev, A. Shivarova, and Kh. Tarnev, J. Phys.: Conf. Series **63**, 012020 (2007).
[35]I. D. Kaganovich and O. Polomarov, Phys. Rev. E **68**, 026411 (2003).
[36]V. Godyak, Plasma Phys. Controlled Fusion **45**, A399 (2003).
[37]M. Bacal, A. M. Bruneteau, W. G. Graham, G. W. Hamilton, and M. Nachman, J. Appl. Phys. **52**, 1247 (1981).
[38]P. Svarnas, J. Bretou, and M. Bacal, Rev. Sci. Instrum. **77**, 03A532 (2006).